

Viscous Withdrawal of Miscible Liquid Layers

Laura E. Schmidt and Wendy W. Zhang

*The Department of Physics & The James Franck Institute,
University of Chicago, Chicago, Illinois 60637, USA*

(Dated: February 6, 2020)

In viscous withdrawal, a converging flow imposed in an upper layer of viscous liquid entrains liquid from a lower, stably stratified layer. Using the idea that a thin tendrils is entrained by a local straining flow, we propose a scaling law for the volume flux of liquid entrained from miscible liquid layers. A long-wavelength model including only local information about the withdrawal flow is degenerate, with multiple tendrils solutions for one withdrawal condition. Including information about the global geometry of the withdrawal flow removes the degeneracy while introducing only a logarithmic dependence on the global flow parameters into the scaling law.

Recent experiments on thermal convection with two layers of miscible liquids reveal several distinct regimes – an overturn regime with violent mixing of the layers, a doming regime where the interface undulates, and a stratified regime where the convection is largely stable with thin tendrils or sheets of one liquid entrained within the other [1]. Analogous steady-state entrained structures arise in drainage flows [2, 3], oil extraction [4], as well as viscous withdrawal of immiscible liquid layers, which occur in microfluidics [5], fiber coating [6] and encapsulation of biological cells [7]. Recent works exploring the connections between thermodynamic phase transitions and the topology transition that takes place at the onset of entrainment have noted that, in order for the entrained structure to be completely isolated from the large-scale flow dynamics, the shape of its base must be a power-law cusp [2, 8, 9, 10]. Intriguingly, experiments [11, 12] on miscible entrainment also seem to show a robust cusp-like shape at the base of long-lived tendrils (see Fig. 1). This suggests the entrained tendrils are isolated from the fluctuating, large-scale convection by the cusp-shaped base and are therefore able to remain stable over many convection cycles. If true, this may even explain why hot-spots can persist over many convection cycles in the Earth’s mantle [12, 13]. Motivated by these observations, we focus on the stratified regime in thermal convection of miscible layers and present a model that tests how the large-scale flow and topography anchor a thin cylindrical tendril.

Because the large-scale flow is stabilized in the stratified regime, mixing between the layers is controlled by the volume flux of liquid entrained through the tendrils, Q_0 . Existing estimates of Q_0 assume that the velocity field inside the tendril is uniformly upwards, flowing at a characteristic convection speed [11, 12, 14]. However, recent particle-image-velocimetry (PIV) measurements within the base of an anchored tendril reveal a stagnation-point velocity field, one more appropriately described by a characteristic strain rate E (s^{-1}) instead of a characteristic velocity scale [15]. Viscous withdrawal experiments on immiscible layers suggest how an interior stagnation point can arise [8]. When the effect of



FIG. 1: Axisymmetric tendrils entrained by a warmer, upwards flow in a 2-layer thermal convection experiment with miscible oils. Convection is driven by heating the bottom of the tank and cooling the top. The lower fluid is less viscous than the upper and the spacing between tendrils is $O(10 \text{ cm})$. The dark vertical line on the left is a thermocouple [13].

the entrainment penetrates deeply into the lower layer, a broad tendril forms with the interior moving uniformly upwards. This is the situation addressed by existing estimates. When the effect of the entrainment penetrates weakly, a narrow tendril forms by drawing liquid inward within a thin layer below the interface, thus creating an interior stagnation point. Here we derive a new scaling law for the volume flux entrained, one which takes into account the interior stagnation point.

The steady-state flow fields associated with non-linear interface deformations are difficult to obtain analytically. We therefore analyze the simplest case: the steady-state entrainment of a tendril from a deep lower layer by an axisymmetric viscous withdrawal flow imposed in an upper layer (Fig. 2). The entrained liquid is taken to be much less viscous than the exterior, so that there is only a weak feedback from entrained flow to the withdrawal flow. To ensure that the effect of entrainment penetrates only weakly into the lower layer, we require that the layers are strongly stratified. With these simplifications, the steady-state interface divides into three geometrically distinct regions: a long and slender entrained tendril where interior flow effects are dominant, a far-field interface where the hydrostatic pressure is dominant, and a transition region where the force balance changes smoothly from one form to another.

First we will give a scaling argument that predicts the volume flux Q_0 . The system is best described by a cylindrical coordinate system where $z = 0$ corresponds to

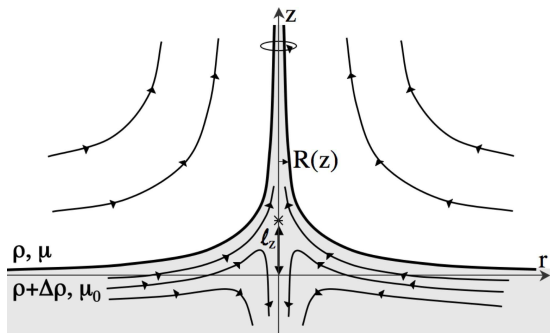


FIG. 2: Sketch of surface $R(z)$ and flow streamlines for an axisymmetric withdrawal flow in the upper liquid layer entraining a thin, cylindrical tendril from a deep lower layer.

the height of the undisturbed interface and $r = 0$ corresponds to the centerline of the tendril. The steady-state tendril radius is defined as $R(z)$. In the strongly stratified regime considered here, the stagnation point inside the tendril lies at a height ℓ_z . The velocity field near the stagnation point is an axisymmetric straining flow, $(-Er/2)\mathbf{e}_r + Ez\mathbf{e}_z$. To estimate Q_0 we note that, above ℓ_z , the liquid from the lower layer is moving entirely upwards so that $Q_0 \approx (Ez)\pi R^2(z)$. Since it is possible to relate ℓ_R , the tendril radius near the stagnation point, to ℓ_z in a simple way described below, the volume flux is $Q_0 \approx (E\ell_z)\pi\ell_R^2$.

Assuming the tendril is long and slender in the neighborhood of the stagnation point, the interior velocity field can be approximated via standard slender body type arguments [16]. The upwards contribution to the interior flow due to entrainment is then a uniform plug flow, Ez . The downward contribution is a pipe flow driven by hydrostatic pressure $\Delta\rho g(R^2(z) - r^2)/(4\mu_0)$, where $\Delta\rho$ is the density difference between the two layers, g the gravitational acceleration, and μ_0 is the viscosity of the entrained liquid. By definition, these two flows must cancel at the interior stagnation point ($r = 0, z = \ell_z$) so that

$$E\ell_z \sim \frac{\Delta\rho g}{4\mu_0} \ell_R^2. \quad (1)$$

It remains to determine ℓ_z . We identify ℓ_z as the amplitude of the large-scale upwards deflection produced on the interface by the withdrawal flow. It is therefore set by a balance of μE , the upwards pull exerted by viscous stresses in the upper-layer withdrawal flow, where μ is the viscosity of the liquid in the upper layer, and $\Delta\rho g$, the downwards pull of hydrostatic pressure. To simplify the notation for later analysis which uses ℓ_z as a characteristic lengthscale, we define

$$\ell_z \equiv 2\mu E / \Delta\rho g. \quad (2)$$

Relations (1) and (2) together yield

$$\ell_R = \sqrt{2 \left(\frac{2\mu_0 E}{\Delta\rho g} \right) \left(\frac{2\mu E}{\Delta\rho g} \right)}, \quad (3)$$

corresponding to the geometric mean of the viscous lengthscale associated with the upper layer flow and the, much smaller, viscous lengthscale associated with the less viscous, lower layer flow. The tendril “slenderness ratio”, ℓ_R/ℓ_z , assumed to be small at the beginning of our analysis, is $\sqrt{2\mu_0/\mu}$, which is indeed small for $\mu_0 \ll \mu$.

Finally, using (1) and (2), we can rewrite Q_0 in terms of the local strain rate E and material parameters

$$Q_0 = 16\pi c_0 \mu^2 \mu_0 E^4 / (\Delta\rho g)^3, \quad (4)$$

where c_0 is an $O(1)$ dimensionless entrainment coefficient which we determine later in the full analysis. This scaling law differs from existing estimates based on a characteristic convection velocity U [11, 12, 14]. If we take S as the size of the convection cell, then (4) says $Q_0 \propto (U/S)^4$ while existing estimates say $Q_0 \propto U^3$. We also emphasize that nothing in the above scaling argument depends on the withdrawal being axisymmetric. An analogous argument for entrained 2-d sheets yields the same relations for ℓ_z (2) and the sheet thickness ℓ_R (3), and the scaling law $Q_0/L \approx E\ell_z\ell_R$ for the volume flux per unit length.

In deriving the scaling law for Q_0 (4) we essentially assumed the entrainment dynamics is controlled by a local straining flow. Since a straining flow has no inherent lengthscale, the dynamics is completely decoupled from the geometry of the large-scale withdrawal flow. In thermal convection, this feature would imply that the volume flux Q_0 has no dependence on the size of the large-scale convection cell. The last implication is counter-intuitive. After all, the tendril size at its base, where it joins on the interface, is controlled by how the interface levels out and becomes flat on the large lengthscales. This large-scale topography in turn depends on the specific geometry of the withdrawal flow, so physical intuition says that the entrainment dynamics, particularly Q_0 , should also depend on the global geometry.

We next address this question by developing a long-wavelength model of the entrainment dynamics and find that a model which includes only the local straining flow is degenerate. For each value of Q_0 , there exists a continuous family of tendril solutions, each with a different power-law shape at the base. The existence of a steady-state tendril thus does not require a specific power-law base shape. Including the large-scale withdrawal flow geometry removes this degeneracy. It also introduces a logarithmic dependence on the global dynamics into the scaling law for Q_0 (4).

Starting with the Navier-Stokes equations, and using standard slender-body approximations where effects proportional to ℓ_R/ℓ_z are discarded at leading-order, we derive the following equation for the steady-state tendril shape

$$Q_0 = (Ez)\pi R^2(z) - \frac{\pi R^4(z)}{8\mu_0} \frac{dP_0}{dz} \quad (5)$$

and interior pressure

$$P_0 = 2\mu E \left(1 + \frac{z}{R(z)} \frac{dR}{dz} \right) + \Delta\rho g z. \quad (6)$$

In essence, equation (5) says that the *unknown* volume flux of liquid entrained into the tendril has two contributions: a plug flow Ez induced by the withdrawal, and a pipe flow associated with non-uniform interior pressure. The expression for P_0 (6) derives from the normal stress balance across the surface of the tendril. The second term is the familiar hydrostatic pressure difference. The first term is the large pressure necessary to keep a tendril from collapsing under the inward squeeze exerted by the exterior straining flow. Equations (5) and (6) together yield a second-order nonlinear ordinary differential equation for the steady-state tendril shape $R(z)$ and Q_0 . The derivation is analogous to the entrainment model for immiscible liquids in [10], except that the surface tension contribution to P_0 is replaced here by the hydrostatic pressure difference.

The natural boundary conditions are conditions on how the tendril shape $R(z)$ tapers to 0 downstream as $z \rightarrow \infty$ and how $R(z)$ flares out into a flat interface upstream as $z \rightarrow 0$. Both conditions correspond to asymptotic balances of the governing equations. Far above the interface, the upwards plug flow Ez dominates and

$$R(z) \rightarrow R_\infty(z) = \sqrt{Q_0(c_0)/(\pi Ez)} \quad \text{as } z \rightarrow \infty, \quad (7)$$

where we have written $Q_0(c_0)$ to emphasize that in our analysis, we use the scaling law (4) for Q_0 , so that c_0 is the only undetermined parameter. Near the tendril base, the effects of entrainment are negligible because the layers are strongly stratified. The tendril base shape is therefore determined by a balance of the hydrostatic pressure and the exterior viscous stress, thus

$$R(z) \rightarrow R_s(z) = B \left(\frac{\ell_z}{z} \right)^\alpha e^{-z/\ell_z} \quad \text{as } z \rightarrow 0. \quad (8)$$

Both the coefficient B and the exponent α are determined self-consistently with the full solution.

Using boundary conditions (7), (8), and appropriate downstream structural stability modes, we numerically integrated equations (5) and (6) for tendril solutions [17]. We found that, for a fixed Q_0 , a continuous family of tendril solutions exist. Each solution's upstream shape is characterized by a different set of B, α values. Fig. 3 gives a few examples of the different tendrils possible for the same volume flux. The long-wavelength model is therefore clearly degenerate.

Removing the degeneracy requires an additional condition on the upstream shape, one related to the large-scale topography. We next show this explicitly. In our toy model an axisymmetric withdrawal flow is generated in the upper layer by inserting a point force with strength

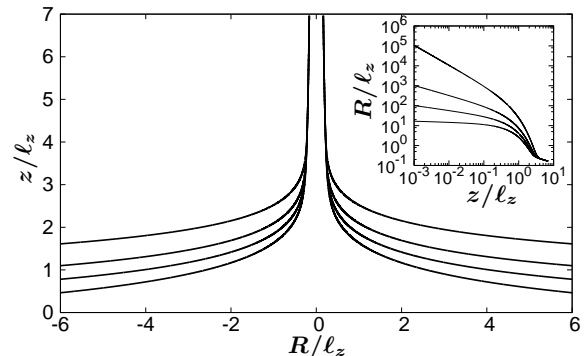


FIG. 3: Rescaled tendril solutions at $S/\ell_z = 15$, $\mu_0/\mu = 0.1$, $c_0 = 3.1$ with exponents $\alpha = 1.0, 0.5, 0.25, 0.052$ (top to bottom). Inset shows tendril solution's power-law divergence.

F at a height S above the undisturbed interface. This is clearly not a realistic withdrawal near the point force but, if S is large, it is a good approximation of realistic withdrawal flows near the interface. The velocity fields in both fluid layers can be obtained by a variation of the method of images [18] and correspond to an axisymmetric straining flow with $E = F/(2\pi\mu S^2)$ in the neighborhood of the base of the tendril. Since the effects of entrainment penetrate weakly into the lower layer, the large-scale interface shape should be well approximated by the deflection occurring when no liquid is entrained,

$$R_I(z) = S \sqrt{(3\ell_z/2z)^{2/5} - 1}. \quad (9)$$

The fact that $R_I(z)$ is controlled by S is the extra information needed to uniquely select a tendril solution.

To incorporate this extra information, we require that at an unknown location z_s , the tendril shape, as well as dR/dz and d^2R/dz^2 equal the corresponding quantities in $R_I(z)$ [19]. We solve for z_s , α and B analytically as follows. Since z_s should be near the base of the tendril, we approximate $R(z)$ by the upstream shape R_s (8) and find that $z_s \approx 0.609 \ell_z$, $\alpha \approx 0.052$, and $B \approx 1.18 S$. We can solve for the appropriate tendril solution numerically by varying the dimensionless entrainment coefficient c_0 so that $R(z)$ and its derivative merge smoothly onto $R_I(z)$. Fig. 4 shows an example of how c_0 is found numerically.

It is interesting to know how the dimensionless entrainment coefficient c_0 depends on the global lengthscale, S/ℓ_z , and on the viscosity contrast μ_0/μ . We have varied S/ℓ_z from 10 to 10^8 and μ_0/μ from 10^{-1} to 10^{-6} and plotted the results in the inset of Fig. 4. The variation of c_0 with these parameters is unexpectedly simple, well approximated by $c_0 = 2.3 \log \left(S/(\ell_z \sqrt{\mu_0/\mu}) \right) - 0.74$. The logarithmic dependencies of c_0 on S/ℓ_z and μ_0/μ are weaker than the power-law dependencies of Q_0 on ℓ_z and μ_0/μ in the scaling law (4). This shows that including the global dynamics only weakly modifies the simple entrainment law.

The logarithmic dependence ultimately results from

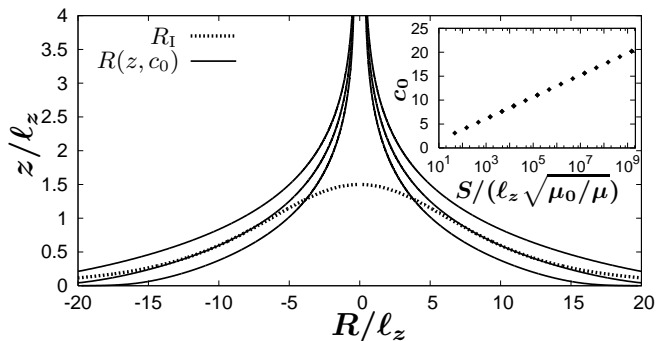


FIG. 4: Rescaled tendril solutions $R(z)$ for $c_0 = 3.4, 3.1$, and 2.9 (solid lines, top to bottom), together with the large-scale deflection solution $R_I(z)$ (dotted) for $S/\ell_z = 15$ and $\mu_0/\mu = 0.1$. Only $c_0 = 3.1$ allows the two shapes to merge smoothly. Inset shows the values of c_0 found from joining the numerical solutions smoothly onto $R_I(z)$ in this way.

the decaying exponential shape of the tendril at $z \sim \ell_z$ (8). How this emerges is complicated because c_0 is essentially determined by demanding $R_\infty(z)$ merge onto $R_s(z)$ through a region where all the terms in the governing equation (5) are equally important. Our rough analysis shows that two requirements appear necessary for the observed c_0 relation. First, the upstream tendril shape $R_s(z)$ should assume a size consistent with $R_\infty(z)$, the steady-state downstream shape. Second, the tapering of the tendril must be accomplished by $z \approx \ell_z$, with the sharp exponential decay in $dR_s(z)/dz$ appropriately switching over to a gentler square-root decay in $dR_\infty(z)/dz$ [17].

In sum, we have now an improved scaling law for Q_0 , one which explicitly accounts for the dependencies on the global flow parameters

$$Q_0 = \frac{16\pi\mu^2\mu_0 E^4}{(\Delta\rho g)^3} \left(\gamma_1 \log \left(\frac{S}{\ell_z \sqrt{\mu_0/\mu}} \right) + \gamma_2 \right), \quad (10)$$

where $\gamma_1 = 2.3$ and $\gamma_2 = -0.74$. We have also analyzed tendril solutions associated with the withdrawal flows generated by a ring vortex and by a point sink and found the same qualitative outcome. The differences in geometry between these withdrawal flows result in slightly different tendril shapes and values of γ_1 and γ_2 . Using (10) we have estimated how quickly two miscible layers will mix in thermal convection and found results consistent with observed values. However, the strong dependence on E of (10) makes a precise comparison difficult. To fully establish how the tendril persists over time, a complete numerical study as well as an experiment where the withdrawal is generated directly, e.g. by withdrawing liquid from a tube inserted into the upper layer [2, 8, 9], instead of indirectly via thermal convection, are needed.

Aside from providing an estimate for Q_0 that takes into account the interior stagnation point, our analysis also reveals that, although some information about the large-scale flow is necessary to specify a tendril shape,

the dependence on the large-scale flow geometry is weak. This may be why tendrils in thermal convection experiments can remain stable over long periods of time despite fluctuations in the global convection which can alter the large-scale topography.

The authors thank Anne Davaille, Sarah C. Case, Leo P. Kadanoff and Sidney R. Nagel for encouragement and helpful discussions. This work was supported by a GAANN Fellowship (L.E.S.) and NSF MRSEC DMR-0213745.

- [1] A. Davaille, *J. Fluid Mech.* **379**, 223 (1999); M. Le Bars and A. Davaille, *J. Fluid Mech.* **499**, 75 (2004).
- [2] S. Courrech du Pont and J. Eggers, *Phys. Rev. Lett.* **96**, 034501 (2006).
- [3] J. T. Jeong and H. K. Moffatt, *J. Fluid Mech.* **241**, 1 (1992).
- [4] S. Blake and G. N. Ivey, *J. Volcanol. & Geotherm. Res.* **27**, 153 (1986); J. R. Lister, *J. Fluid Mech.* **198**, 231 (1989).
- [5] A. M. Gañán Calvo, M. Perez-Saborid, J. M. Lopez-Herrera, and J. M. Gordillo, *Eur. Phys. J. B* **39**, 131 (2004); R. Suryo and O. A. Basaran, *Phys. Fluids* **18**, 082102 (2006); S. L. Anna, N. Bontoux, and H. A. Stone, *Appl. Phys. Lett.* **82**, 364 (2003).
- [6] P. G. Simpkins and V. J. Kuck, *Nature* **403**, 641 (2000); J. Eggers, *Phys. Rev. Lett.* **86**, 4290 (2001); E. Lorenceau, F. Restagno, and D. Quéré, *Phys. Rev. Lett.* **90**, 184501 (2003); E. Lorenceau, D. Quéré, and J. Eggers, *Phys. Rev. Lett.* **93**, 254501 (2004).
- [7] I. Cohen, H. Li, J. L. Houglund, M. Mrksich, and S. R. Nagel, *Science* **292**, 265 (2001); J. L. Wyman, S. Kizilel, R. Skarbek, X. Zhao, M. Connors, W. S. Dillmore, W. L. Murphy, M. Mrksich, and S. R. Nagel, *Small* **3**, 683 (2007).
- [8] S. C. Case and S. R. Nagel, *Phys. Rev. Lett.* **98**, 114501 (2007).
- [9] I. Cohen and S. R. Nagel, *Phys. Rev. Lett.* **88**, 074501 (2002).
- [10] W. W. Zhang, *Phys. Rev. Lett.* **93**, 184502 (2004).
- [11] A. M. Jellinek and M. Manga, *Nature* **418**, 760 (2002).
- [12] A. Davaille, F. Girard, and M. Le Bars, *Earth Planet. Sci. Lett.* **203**, 621 (2002).
- [13] A. M. Jellinek and M. Manga, *Rev. Geophys.* **42**, RG3002 (2004).
- [14] N. H. Sleep, *Geophys. J.* **95**, 437 (1988).
- [15] A. Davaille, Poster, Focusing Stress in a Soft Interface Workshop, U. Chicago (2005).
- [16] A. Acrivos and T. S. Lo, *J. Fluid Mech.* **86**, 641 (1978); G. I. Taylor, *Proc. Int. Congr. Appl. Mech. Munich* **11**, 191 (1964).
- [17] L. E. Schmidt and W. W. Zhang, unpublished.
- [18] S. H. Lee, R. S. Chadwick, and L. G. Leal, *J. Fluid Mech.* **93**, 705 (1979).
- [19] Here we have chosen the simpler option of matching $R_I(z)$ and $R(z)$ at a point instead of systematically matching them. Our numerics show the tendril merges smoothly onto $R_I(z)$, so the errors appear small. The simpler procedure also has the advantage of revealing parameter dependencies in an explicit way.